nature chemistry

ARTICLES

PUBLISHED ONLINE: 22 JANUARY 2018 | DOI: 10.1038/NCHEM.2926

Endothermic singlet fission is hindered by excimer formation

Cameron B. Dover[1†], Joseph K. Gallaher[1†], Laszlo Frazer[1], Patrick C. Tapping[2], Anthony J. Petty II[3], Maxwell J. Crossley[4], John E. Anthony[3], Tak W. Kee[2] and Timothy W. Schmidt[1*]

Singlet fission is a process whereby two triplet excitons can be produced from one photon, potentially increasing the efficiency of photovoltaic devices. Endothermic singlet fission is desired for a maximum energy-conversion efficiency, and such systems have been considered to form an excimer-like state with multiexcitonic character prior to the appearance of triplets. However, the role of the excimer as an intermediate has, until now, been unclear. Here we show, using 5,12-bis ((triisopropylsilyl)ethynyl)tetracene in solution as a prototypical example, that, rather than acting as an intermediate, the excimer serves to trap excited states to the detriment of singlet-fission yield. We clearly demonstrate that singlet fission and its conjugate process, triplet–triplet annihilation, occur at a longer intermolecular distance than an excimer intermediate would impute. These results establish that an endothermic singlet-fission material must be designed to avoid excimer formation, thus allowing singlet fission to reach its full potential in enhancing photovoltaic energy conversion.

Singlet fission (SF) is a process whereby a photogenerated singlet exciton splits into two spin-correlated triplet excitons[1,2], which can occur when the triplet exciton has about half the energy of the singlet exciton and there is suitable coupling between two chromophores[3–9]. This is of current interest as it offers the possibility to circumvent the Shockley–Queisser limit of single-threshold solar cells, such as those based on crystalline silicon (c-Si), but its detailed mechanism is a matter of some debate[4,6,10–18]. Exothermic SF, in which the energy of two triplet excitons is lower than that of the initial singlet exciton, has been shown to proceed rapidly with high yields, and has been incorporated into prototypical devices[19–22]. However, the resulting triplet states are too low in energy to be coupled to existing efficient photovoltaic cells. Indeed, it has been shown that the most-efficient SF solar cell should exhibit fission that is endothermic, energetically 'uphill', corresponding to an upper-energy conversion-efficiency limit of 45.9% (refs 23,24). In principle, SF is applicable to any semiconductor material, be it c-Si, perovskite or chalcogenide.

One class of chromophore that exhibits endothermic fission is the tetracene derivatives. These are especially interesting for potential solar energy applications because their triplet energies (~1.2 eV) are slightly above the bandgap of silicon (1.12 eV), offering the possibility to boost significantly the efficiency of c-Si cells. However, the exciton dynamics of tetracene are far from straightforward[9,13,25–28].

Tetracene films exhibit a rapid dimming of photogenerated singlet excitons with a time constant of about 80 ps (refs 25,26,29). However, although this has been associated with SF, it has been demonstrated to have no significant temperature dependence, despite its endothermic nature. This has necessitated the invocation of a lower-energy, spectroscopically dim intermediate state[25,30]. At low temperatures, this 'intermediate' is trapped, and results in bathochromically shifted excimer-like emission[25,30].

The idea that endothermic emission proceeds via an excimer of multiexcitonic character is supported by a report of transient absorption (TA) spectroscopy in high-concentration solutions of 5,12-bis((triisopropylsilyl)ethynyl)tetracene (TIPS-Tc). Friend and co-workers[31] reported that the excimer exhibits a TA spectrum much closer in appearance to the triplet state than the excited singlet, which implies its role as an intermediate in SF. This idea has also been invoked by Mauck *et al.*, who identified excimer-like

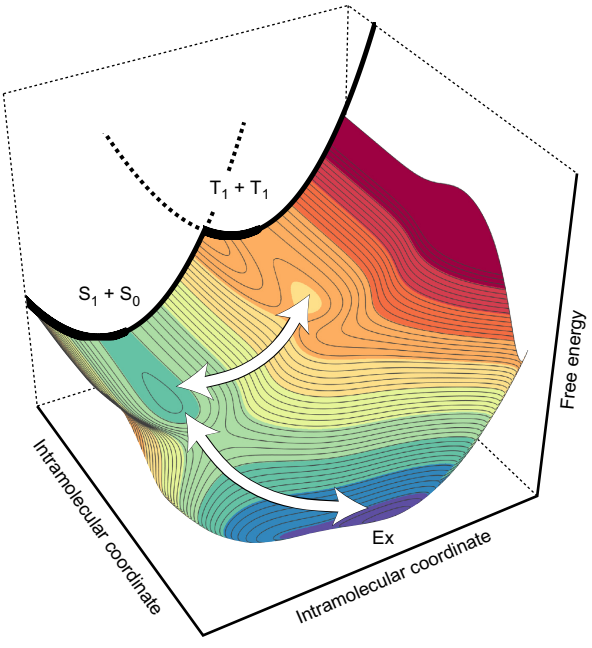

Figure 1 | Schematic Marcus–Hush–Morse free-energy surface of the SF–TTA process. The intramolecular coordinate interconverts singlet and triplet chromophore geometries. The intermolecular coordinate represents the distance and disposition of the two chromophores. In this model, the tightly bound excimer state (Ex) may have $T_1 \cdots T_1$ character, yet the route to free $T_1 + T_1$ is via $S_1 + S_0$. TTA populates $S_1 + S_0$ (Supplementary Information gives the mathematical details of surface construction.).

[1]ARC Centre of Excellence in Exciton Science, School of Chemistry, UNSW Sydney, NSW 2052, Australia. [2]Department of Chemistry, The University of Adelaide, SA 5005, Australia. [3]Department of Chemistry, University of Kentucky, Lexington, Kentucky 40506, USA. [4]School of Chemistry, The University of Sydney, NSW 2006, Australia. [†]These authors contributed equally to this work. *e-mail: timothy.schmidt@unsw.edu.au

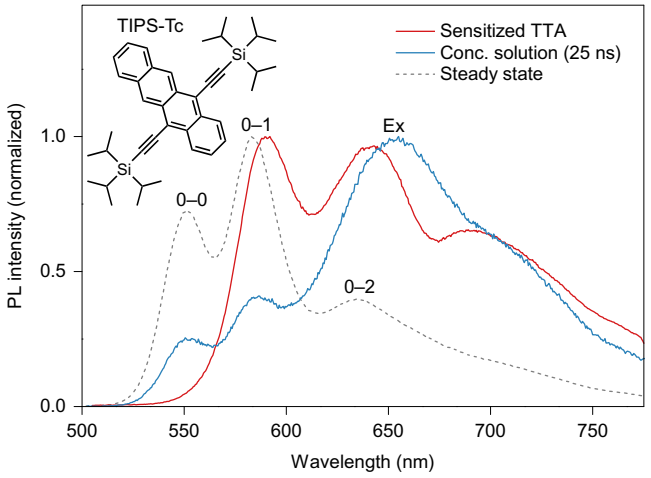

Figure 2 | Emission spectra of concentrated TIPS-Tc solutions. The concentrated solution at 25 ns is dominated by an excimer contribution (Ex), whereas both the sensitized-TTA and steady-state spectra display prominent S_1 (0-1) features, which implies that TTA does not proceed via an excimer intermediate. The sensitized-TTA spectrum is influenced by the absorption spectrum of the sensitizer ($PdPQ_4$, see Supplementary Information).

precursors to SF in thin films of diketopyrrolopyrrole using transient optical spectroscopy[32]. These reports clash with a recent theoretical study on the electronic coupling between tetracene motifs that predicts excimer geometries have an increased coupling to the ground state and increased rate of radiationless relaxation; therefore, the formation of an excimer may, in fact, be detrimental to SF[12,33]. This view is supported by studies of isomorphs of 1,3-diphenylisobenzofuran, which argue that excimer formation hinders SF[34,35].

If the excimer were an intermediate to SF, it must also be observed to the same extent in the reverse process, triplet–triplet annihilation (TTA)[36]. In this report, we clearly demonstrate that this is not the case, and that a model of the time-resolved photoluminescence (TRPL) is not consistent with an excimer intermediate. Rather, SF results primarily from a direct pathway with the excimer acting as a trap, as illustrated in Fig. 1. This has important implications for the design of endothermic SF materials: excimer formation is to be avoided, as it does not aid in the SF process, but rather hinders it.

Results

Figure 2 (red trace) displays the time-integrated photoluminescence (PL) that results from sensitized TTA in a concentrated TIPS-Tc solution (180 mg ml^{-1}). The most-intense peak corresponds to the 0–1 emission band of the S_1 state of TIPS-Tc, with the 0–0 band suppressed by self-absorption and by the triplet sensitizer, a palladium porphyrin (Supplementary Information gives the details of the modelling of reabsorption). As the sample was irradiated by a 670 nm laser pulse, the upconverted TIPS-Tc PL at shorter wavelengths results from annihilation of TIPS-Tc triplets (T_1). In PL studies of concentrated TIPS-Tc solutions, in which the S_1 state is directly excited at 500 nm, the emission rapidly takes on the appearance of an excimer, which has been reported by Friend and co-workers to be of multiexcitonic character[31]. The emission spectrum of a concentrated TIPS-Tc solution, 25 ns after excitation, is shown as the blue trace in Fig. 2. The disparity between these spectra (red and blue traces in Fig. 2) is striking, and shows that the TTA process, which is the conjugate of SF, does not efficiently regenerate the excimer spectrum. To see if this is also true of SF-generated triplets, we performed a TRPL study of a concentrated TIPS-Tc solution, the results of which are plotted in Fig. 3.

A heat map of the TRPL as a function of wavelength and time is displayed in Fig. 3a. At very early times, the emission appears to be dominated by free S_1-state TIPS-Tc molecules, as shown in Fig. 3b (red trace). This rapidly transmutes into an excimer-dominated spectrum that persists out to 50 ns after laser excitation. The 25 ns spectrum, shown Fig. 3b, clearly exhibits residual S_1 emission evidenced by the 0–0 and 0–1 emission bands. At times longer than 50 ns, the emission again becomes dominated by S_1 emission. This is consistent with a long-time emission caused by TTA which, as shown by the sensitized TTA experiments, generates a spectrum dominated by S_1 emission. An understanding of the interplay between the various states in this system necessitates a kinetic model.

Discussion

In the following, the rate constant for the forward process is given above the equilibrium arrows and the rate constant for the reverse process is given below. The photogenerated S_1 states pair with ground state S_0 molecules to generate excimers (Ex) on a picosecond timescale:

$$S_1 + S_0 \underset{k_1'}{\overset{k_1}{\rightleftharpoons}} Ex \quad (1)$$

The excimers are considered to dissociate to yield free triplets:

$$Ex \underset{k_2'}{\overset{k_2}{\rightleftharpoons}} T_1 + T_1 \quad (2)$$

Then, as shown by our TTA experiments, there must exist a channel that directly links the free triplets with the S_1 manifold:

$$T_1 + T_1 \underset{k_3'}{\overset{k_3}{\rightleftharpoons}} S_1 + S_0 \quad (3)$$

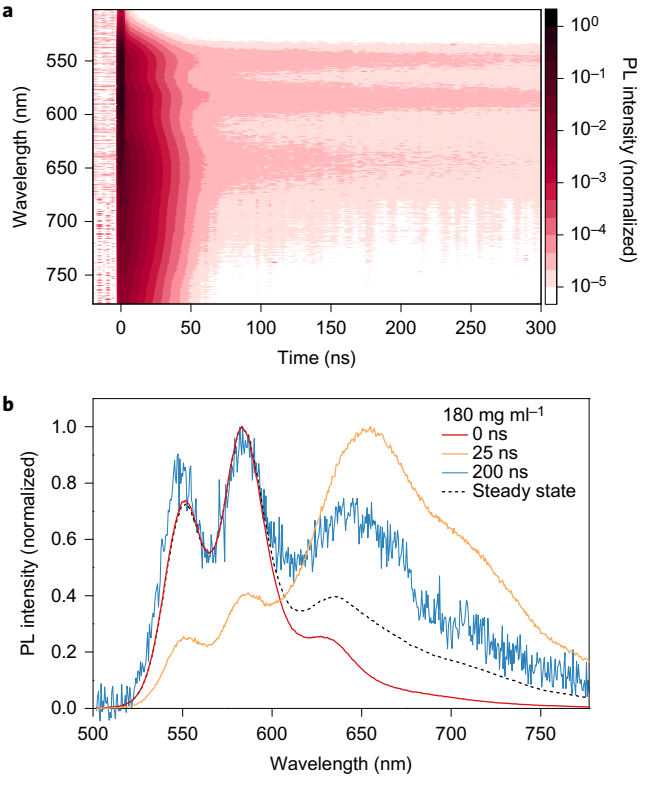

Figure 3 | TRPL of concentrated TIPS-Tc in toluene. The emission spectrum reverts to being dominated by the S_1 state after excimer decay. **a**, Heat map of TRPL after pumping to S_1. **b**, Spectral slices illustrating the spectral dynamics.

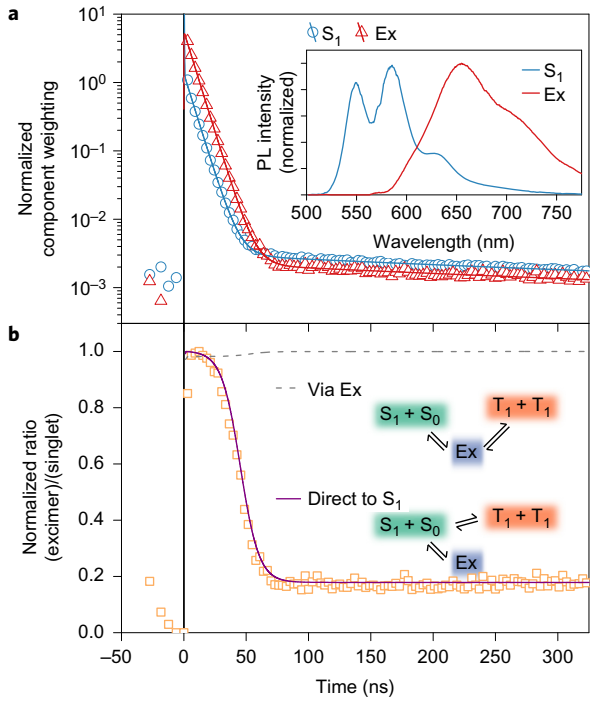

Figure 4 | Extracted spectra and their time-dependent weightings. **a**, Multivariate curve resolution–alternating least squares-extracted S_1 and excimer emission components as a function of time after pumping to S_1 (inset, spectral components). **b**, The evolution of the Ex:S_1 ratio with time. The grey dashed line is the result of a fit with a model that only incorporates fission via the excimer state (Supplementary Information). The solid lines are the results of a fit with a model that only incorporates direct fission from S_1. The time-zero data point has been cropped as the time resolution of the TRPL (3 ns) is insufficient to resolve the prompt initial decay of the S_1 population.

We assume that re-absorption does not play a significant role in the excitonic kinetics and that it only serves to modify the appearance of spectra.

In the above processes, to satisfy the principle of detailed balance, each reverse process must balance the forward process such that the change in Gibbs energy is $\Delta G_i = -k_B T \log(k_i/k_i')$. The cyclic nature of the above processes constrains the overall changes in Gibbs energy such that $\Delta G_1 + \Delta G_2 + \Delta G_3 = 0$. The states S_1, Ex and T_1 decay (non)-radiatively to S_0 with rate constants of k_S, k_{Ex} and k_T.

The TRPL in Fig. 3 was fit with two independent spectra, with time-varying amplitudes, to extract the time dependence of the S_1 and Ex concentrations. All wavelengths were used in the fit. The results of this procedure are shown in Fig. 4a. It is important to note that the time-zero data point has been excluded from Fig. 4 as the time resolution of the TRPL (3 ns) is insufficient to resolve the initial picosecond decay of the S_1 population (Supplementary Information describes the optically gated TRPL experiments). The extracted spectral weightings at time zero have $S_1 > Ex$ (Supplementary Fig. 8), but within the 3 ns time resolution the excimer state becomes dominant. The ratios of the Ex and S_1 weightings are approximately constant for this initial time period ($\lesssim$25 ns). After 25 ns, the ratio of Ex to S_1 plummets (Fig. 4b), and the S_1 spectrum once again becomes dominant after 65 ns. From 100 ns, the ratio of the Ex and S_1 weightings is again constant, with both spectra decaying with a long time constant.

We applied several kinetic models in an attempt to reproduce the observed data. In the 'sequential' model, we constrained k_3 and k_3' to be zero, and fixed k_1, k_S and k_T from the results of TRPL experiments (Supplementary Fig. 12). The free kinetic parameters are thus k_1', k_2, k_2' and k_{Ex}. Unsurprisingly, this model completely fails to capture the essence of the TRPL. The results are shown as a grey dashed curve in Fig. 4b. Without the direct recombination channel (k_3, TTA), the ratio of Ex to S_1 cannot fall below that initially established with the $S_1 + S_0 \rightleftharpoons Ex$ equilibrium.

A second 'parallel' model, which constrains k_2 and k_2' to be zero but allows direct SF (rate k_3') and TTA (k_3), fits the data admirably, as shown by the solid lines in Fig. 4a,b. The initial decay is described by an equilibrium between S_0 and Ex while the population of T_1 increases due to a direct fission mechanism (k_3'), and both S_1 and Ex states decay. After a sufficient build-up of the T_1 population, it becomes the dominant source of the nascent S_1 state molecules. This is accompanied by a change in the emission spectrum and the time constant, now controlled by the T_1 lifetime. The latter is determined here to be about 60 µs. The physicality of this model can be tested by inspecting the ratios k_1/k_1' and k_3/k_3', which result in $\Delta G_1 = -0.13$ eV and $\Delta G_3 = -0.08$ eV. Both have the appropriate sign, though ΔG_3 is a little smaller in magnitude than expected.

The parallel model predicts that the spectrum caused by TTA would be identical to the quasi-steady-state spectrum. However, comparison of the blue and dashed curves in Fig. 3b shows this not to be the case. The apparent excess excimer content in the TTA spectrum (Fig. 3b, blue line) compared with the quasi-steady state suggests that TTA can, indeed, lead to excimer formation. To account for this requires the introduction of rates k_2 and k_2' into the parallel model. The results of a simultaneous fit to the time-resolved and steady-state data are shown in Supplementary Fig. 14. The fit is practically identical to that for the parallel model, with many rate constants unchanged (Supplementary Table 1). The fitted k_2 value is $8.08 \times 10^5\ s^{-1}$, which is about 7% the value of k_1'. This indicates that excimers dissociate into free singlets 14 times more often than they undergo SF.

Our modelling indicates that 84% of the triplets are formed in the first 500 ps, as the S_1 state decays. As such, it cannot be argued that the excimer facilitates SF. Indeed, eight times as many triplets are generated directly from S_1 as from the excimer. By artificially cutting off the excimer formation, we find that the calculated triplet-yield increases substantially.

It may be reasoned that direct dissociation of the excimer state as the dominant path to triplets is unphysical. The observed decay of the excimer state, which controls the first time constant in Fig. 4, has a total rate that exceeds $10^8\ s^{-1}$. Thus, for the excimer state to dissociate into a significant population of triplets, k_2 must exceed $\sim 10^7\ s^{-1}$. However, given that ΔG_2 must be at least 0.2 eV, the TTA rate constant k_2' would exceed the diffusion limit by several times. As such, it is absolutely clear that the SF channel is dominated by a direct mechanism from the S_1 state, and that the excimer state serves to trap the excited-state population.

The question remains how the TA data of Stern *et al.* leads to a different conclusion, that is, the excimer is an intermediate rather than a trap[31]. In their analysis of TA data, Stern *et al.* were able to unambiguously extract signals from the isolated S_1 states and the isolated T_1 states from the TA signal at very early and very late times, respectively, when these species dominate. However, there is no time at which the excimer exists in isolation. After laser excitation, concomitant with S_1 decay, a new absorption profile grows in, which is attributed by Stern *et al.* to the excimer. However, because triplet and excimers grow in at a constant ratio (in our model), these two TA spectra cannot be disentangled. By attributing the absorption profile that grows in immediately after excitation to the excimer alone, the subsequent modelling is biased. Indeed, Stern *et al.* only account for the T_1 population after about 500 ps, when the excimer population is on the decline and the T_1:Ex ratio is increasing[31]. Instead, as shown in Supplementary Information, if the excimer is assumed to grow in working backwards in time, one obtains a rather featureless excimer TA spectrum, and triplets are required to fit the TA data across the transient, in agreement with the present model.

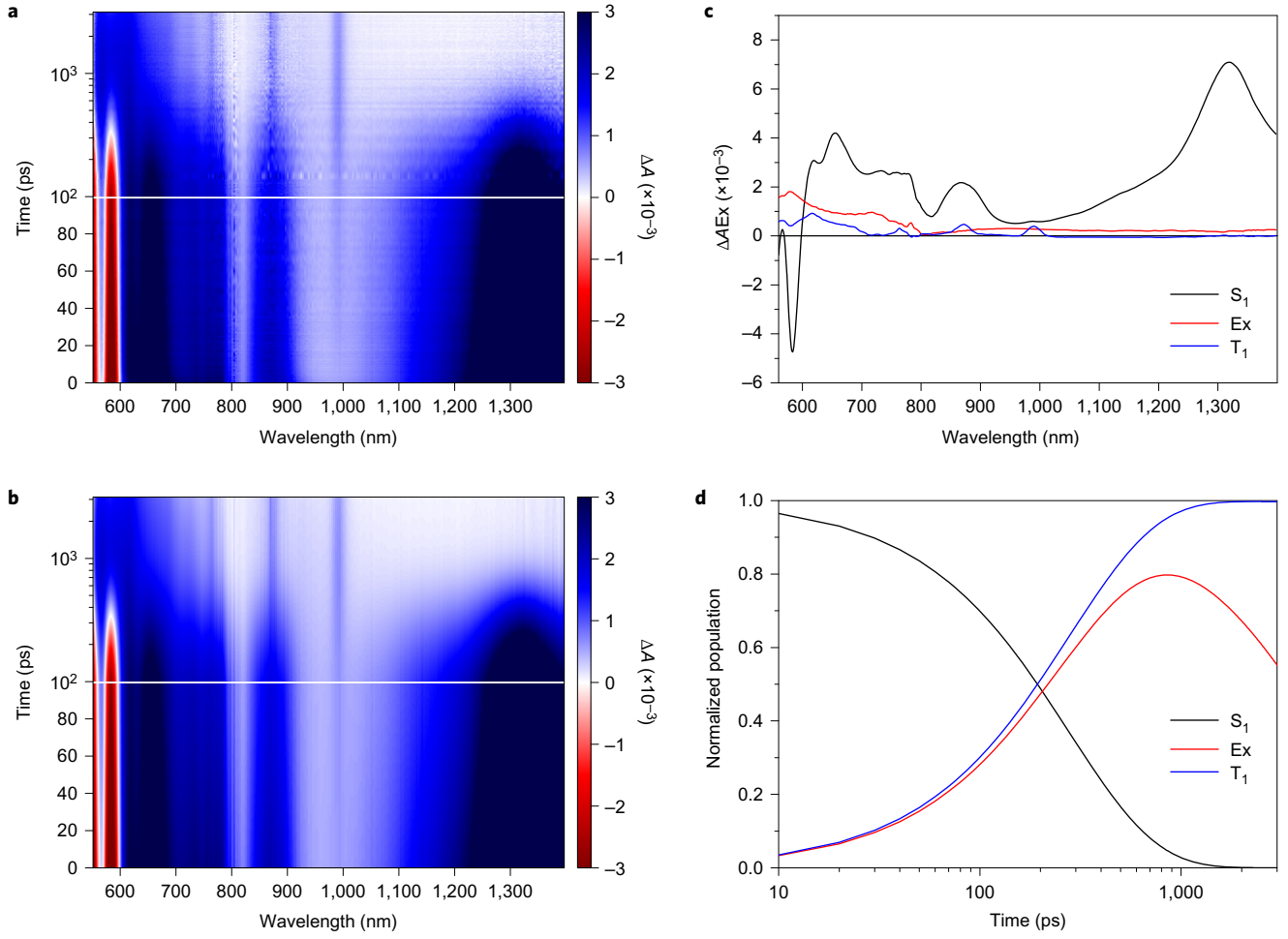

Figure 5 | Experimental and simulated TA heat maps with extracted spectra and time dependences. The data fit well with the three components of time dependences given by an analytic approximation to the parallel model (equation (4)). **a**, TA spectrum of concentrated TIPS-tetracene solution. **b**, Synthetic TA spectrum fit with the three components. The horizontal white lines in **a** and **b** indicate the break between the linear and log time axes. **c**, Derived transient spectra from equation (4). **d**, Transient populations from equation (4).

The results of our own TA experiment are shown in Fig. 5a. Visual inspection reveals at least two components, one that decays and one that grows in. The features that decay may be attributed to the photo-prepared S_1 state, which exhibits stimulated emission features (<600 nm) as well as prominent absorption features (660 and 1,300 nm). The features that grow in are very different, with sharp absorptions that correspond to the features attributed to both T_1 states and excimers by Stern *et al.*[31] Careful analysis reveals three components, with two resolvable time constants. We fit each wavelength independently to an analytical expression corresponding to the parallel mechanism. The function comprises a component that decays with time constant τ_1 (S_1), one that grows in with τ_1 and decays with τ_2 (Ex) and one that grows in with τ_1 but does not decay on the 3 ns timescale (T_1),

$$A(\lambda, t) = S_1(\lambda)\exp\left(\frac{-t}{\tau_1}\right) + \mathrm{Ex}(\lambda)\left[\exp\left(\frac{-t}{\tau_2}\right) - \exp\left(\frac{-t}{\tau_1}\right)\right] + T_1(\lambda)\left[1 - \exp\left(\frac{-t}{\tau_1}\right)\right] \quad (4)$$

where $A(\lambda, t)$ is the time- and wavelength-dependent absorption signal. Each wavelength was fit to this model and the resulting spectra then used to refine the time constants. We alternated between refining the spectra and the time constants to arrive at a converged solution. The results of this procedure are shown in Fig. 5b, with derived spectra in Fig. 5c and time-dependent weightings in Fig. 5d. The parallel mechanism is clearly able to reproduce the observations. Moreover, the derived spectra reveal the Ex TA spectrum to be rather featureless, without the sharper peaks evident at 850 and 980 nm that characterize the T_1 spectrum. By replacing the time dependence of $T_1(\lambda)$ with a function that corresponds to the sequential model (Supplementary equation (10)), an equally valid fit is obtained whereby the Ex spectrum, indeed, exhibits the 850 and 980 nm peaks (Supplementary Fig. 16). The synthetic data are identical because each wavelength is fit to the same effective function: $A(\lambda, t) = a(\lambda)\exp(-t/\tau_1) + b(\lambda)\exp(-t/\tau_2) + c(\lambda)$. The identically valid fits underline that TA spectroscopy alone is unable to distinguish between the two mechanisms.

In films of multicrystalline tetracene, it has been widely assumed that the initial singlet exciton PL decay is associated with decay to a dull intermediate to SF[25,30]. At low temperatures this is evidenced by a redshifted excimer-like emission. However, as in the present case, the delayed fluorescence, which is associated with TTA, is dominated by singlet excitons[25]. The behaviour of multicrystalline tetracene is thus consistent with the present findings that the excimer-like state serves as a trap, and does not facilitate SF.

The implications for the design of endothermic fission materials are clear. As the excimer has a very low fission rate, and its population naturally exceeds that of the fissionable S_1 state after

equilibration, the excimer state is undesirable. It traps population and thus attenuates SF, which must then compete against the decay of the excimer state. As cofacial π-chromophores are liable to exhibit excimer formation, we argue that these cannot be efficient endothermic SF systems. Rather, for efficient endothermic fission to be realised, $\pi-\pi$ interactions must be controlled. To achieve this will enable SF to reach its full potential in enhancing the energy-conversion efficiency of photovoltaic devices.

Methods

All chemicals were purchased from Sigma-Aldrich and used as received, unless otherwise stated. The detailed synthetic procedures for tetrakisquinoxalinoporphyrin (PQ_4Pd) and TIPS-Tc are reported in previous papers[37,38].

To prepare samples for optical spectroscopy, neat solutions of TIPS-Tc and solutions blended with PQ_4Pd were prepared under a nitrogen atmosphere inside a glovebox (MBRAUN MB-UNIlab (1800/780)) to ensure the exclusion of oxygen. The internal environment was maintained to <0.5 ppm O_2. TIPS-tetracene (60.0 mg) and PQ_4Pd (0.158 mg) were dissolved in anhydrous toluene (Sigma-Aldrich), which was used for all the solutions. TIPS-Tc was dissolved in 300 µl of toluene and stirred for 3 h to yield a stock concentration of 200 mg ml^{-1}. PQ_4Pd was dissolved in 100 µl of toluene, also stirred for 3 h, to make a stock concentration of 1.58 mg ml^{-1}. There were no visible solids after 3 h of stirring. To make a neat solution of TIPS-Tc for the spectroscopy experiments, nine parts of the 200 mg ml^{-1} stock were combined with one part of toluene to produce the desired concentration solution of 180 mg ml^{-1}. Sensitized TTA solutions of TIPS-Tc:PQ_4Pd were prepared in the same way, except the one-part toluene was replaced with a one-part PQ_4Pd stock solution. This resulted in a solution of 180 mg ml^{-1} TIPS-tetracene with 0.158 mg ml^{-1} PQ_4Pd. Mechanical agitation was used to ensure mixing of the final solutions. All the samples for time-resolved measurements were sealed in a quartz cuvette before removal from the glovebox.

All samples used for TRPL spectroscopy were measured under an inert atmosphere using a Teflon-stopcock sealed quartz cuvette with a 1 mm path length. TRPL spectroscopy was carried out using a Clark-MXR CPA 2210 150 fs regeneratively amplified titanium-doped sapphire laser operated at a repetition rate of 1 kHz and fundamental wavelength of 780 nm. This was used to drive a Light Conversion TOPAS-C optical parametric amplifier to produce excitation pulses used in two different TRPL techniques.

For ultrafast (<1 ns) measurements, PL was recorded using an Ultrafast Systems Halcyone PL upconversion system with the measurement geometry such that the excitation and detection were from the same face of the cuvette. The optical parametric amplifier was used to produce 500 nm pulses for excitation. The beam was filtered through a band-pass filter (centre 510 nm, width 42 nm) and rotated to the 'magic angle' polarization using a waveplate. The resulting PL was collected and then passed through a β-barium borate (BBO) crystal to generate the sum frequency with the laser fundamental output (780 nm). The sum frequency was filtered using a dielectric band-pass filter (centre 320 nm, width 40 nm) and a double monochromator, and recorded with a photomultiplier tube detector. The excitation power was adjusted using neutral density filters, which confirmed that the picosecond PL dynamics were independent of excitation density. The sample was excited with a maximum of 3.8 µJ cm^{-2} using a laser spot of radius 0.76 mm measured to $1/e^2$.

For other TRPL measurements (nano- to microseconds), an optical parametric amplifier (TOPAS) was used to produce excitation pulses of either 480 or 670 nm. These were selected depending on the experiments, as stated in the text (for example, 670 nm for TTA measurements). The excitation beam was filtered to remove any residual laser fundamental and the excitation power was attenuated using neutral density filters. The sample was excited with 100 µJ cm^{-2} using a laser spot of radius 0.59 mm measured to $1/e^2$. Sample PL was collected from approximately 30° off-axis using concave mirrors, and coupled into a spectrograph (Princeton Instruments 2300i) equipped with a 300 groove mm^{-1} grating blazed at 500 nm, and an intensified time-gated camera (Princeton Instruments PM4-256f-HR-FG-18-P43-SM).

Time-resolved absorption experiments were performed on a TA spectrometer (Ultrafast Systems) at the University of Adelaide. Laser pulses originated from the output of a Ti:sapphire regenerative amplifier (Spectra Physics, Spitfire Pro XP 100F) and provided pulses centred at 800 nm with a 100 fs duration and a 1 kHz repetition rate. Light (400 nm) was produced through second-harmonic generation in a 0.5 mm BBO crystal. The 400 nm pump pulses had an energy of 0.75 µJ with a spot size on the sample of 490 µm full-width at half-maximum. The probe light was produced by focusing a small portion of the 800 nm amplifier output onto a 3.2 or 12.7 mm sapphire crystal for the visible region or near-infrared region (NIR), respectively. The white-light continuum was split into signal and reference beams, and focused onto the sample with a spot size of 225 µm for the visible and 100 µm for the NIR.

Data availability. The data that support the findings of this study are available from the corresponding author on reasonable request.

Received 9 June 2017; accepted 5 December 2017; published online 22 January 2018

References

1. Smith, M. B. & Michl, J. Recent advances in singlet fission. *Annu. Rev. Phys. Chem.* **64,** 361–386 (2013).
2. Smith, M. B. & Michl, J. Singlet fission. *Chem. Rev.* **110,** 6891–6936 (2010).
3. Chan, W.-L. *et al.* Observing the multiexciton state in singlet fission and ensuing ultrafast multielectron transfer. *Science* **334,** 1541–1545 (2011).
4. Walker, B. J., Musser, A. J., Beljonne, D. & Friend, R. H. Singlet exciton fission in solution. *Nat. Chem.* **5,** 1019–1024 (2013).
5. Yost, S. R. *et al.* A transferable model for singlet-fission kinetics. *Nat. Chem.* **6,** 492–497 (2014).
6. Zimmerman, P. M., Zhang, Z. & Musgrave, C. B. Singlet fission in pentacene through multi-exciton quantum states. *Nat. Chem.* **2,** 648–652 (2010).
7. Zirzlmeier, J. *et al.* Singlet fission in pentacene dimers. *Proc. Natl Acad. Sci. USA* **112,** 5325–5330 (2015).
8. Pensack, R. D. *et al.* Observation of two triplet-pair intermediates in singlet exciton fission. *J. Phys. Chem. Lett.* **7,** 2370–2375 (2016).
9. Morrison, A. F. & Herbert, J. M. Evidence for singlet fission driven by vibronic coherence in crystalline tetracene. *J. Phys. Chem. Lett.* **8,** 1442–1448 (2017).
10. Zimmerman, P. M., Bell, F., Casanova, D. & Head-Gordon, M. Mechanism for singlet fission in pentacene and tetracene: from single exciton to two triplets. *J. Am. Chem. Soc.* **133,** 19944–19952 (2011).
11. Chan, W.-L., Ligges, M. & Zhu, X.-Y. The energy barrier in singlet fission can be overcome through coherent coupling and entropic gain. *Nat. Chem.* **4,** 840–845 (2012).
12. Feng, X. & Krylov, A. I. On couplings and excimers: lessons from studies of singlet fission in covalently linked tetracene dimers. *Phys. Chem. Chem. Phys.* **18,** 7751–7761 (2016).
13. Burdett, J. J. & Bardeen, C. J. Quantum beats in crystalline tetracene delayed fluorescence due to triplet pair coherences produced by direct singlet fission. *J. Am. Chem. Soc.* **134,** 8597–8607 (2012).
14. Monahan, N. & Zhu, X.-Y. Charge transfer-mediated singlet fission. *Annu. Rev. Phys. Chem.* **66,** 601–618 (2015).
15. Bakulin, A. A. *et al.* Real-time observation of multiexcitonic states in ultrafast singlet fission using coherent 2D electronic spectroscopy. *Nat. Chem.* **8,** 16–23 (2015).
16. Musser, A. J. *et al.* Evidence for conical intersection dynamics mediating ultrafast singlet exciton fission. *Nat. Phys.* **11,** 352–357 (2015).
17. Busby, E. *et al.* A design strategy for intramolecular singlet fission mediated by charge-transfer states in donor–acceptor organic materials. *Nat. Mater.* **14,** 426–433 (2015).
18. Monahan, N. R. *et al.* Dynamics of the triplet-pair state reveals the likely coexistence of coherent and incoherent singlet fission in crystalline hexacene. *Nat. Chem.* **9,** 341–346 (2016).
19. Ehrler, B. *et al. In situ* measurement of exciton energy in hybrid singlet-fission solar cells. *Nat. Commun.* **3,** 1019 (2012).
20. Ehrler, B., Wilson, M. W. B., Rao, A., Friend, R. H. & Greenham, N. C. Singlet exciton fission-sensitized infrared quantum dot solar cells. *Nano Lett.* **12,** 1053–1057 (2012).
21. Congreve, D. N. *et al.* External quantum efficiency above 100% in a singlet-exciton-fission-based organic photovoltaic cell. *Science* **340,** 334–337 (2013).
22. Tritsch, J. R., Chan, W.-L., Wu, X., Monahan, N. R. & Zhu, X.-Y. Harvesting singlet fission for solar energy conversion via triplet energy transfer. *Nat. Commun.* **4,** 2679 (2013).
23. Tayebjee, M. J. Y., McCamey, D. R. & Schmidt, T. W. Beyond Shockley–Queisser: molecular approaches to high-efficiency photovoltaics. *J. Phys. Chem. Lett.* **6,** 2367–2378 (2015).
24. Tayebjee, M. J. Y., Gray-Weale, A. A. & Schmidt, T. W. Thermodynamic limit of exciton fission solar cell efficiency. *J. Phys. Chem. Lett.* **3,** 2749–2754 (2012).
25. Tayebjee, M. J. Y., Clady, R. G. C. R. & Schmidt, T. W. The exciton dynamics in tetracene thin films. *Phys. Chem. Chem. Phys.* **15,** 14797 (2013).
26. Wilson, M. W. B. *et al.* Temperature-independent singlet exciton fission in tetracene. *J. Am. Chem. Soc.* **135,** 16680–16688 (2013).
27. Arias, D. H., Ryerson, J. L., Cook, J. D., Damrauer, N. H. & Johnson, J. C. Polymorphism influences singlet fission rates in tetracene thin films. *Chem. Sci.* **7,** 1185–1191 (2016).
28. Piland, G. B. & Bardeen, C. J. How morphology affects singlet fission in crystalline tetracene. *J. Phys. Chem. Lett.* **6,** 1841–1846 (2015).
29. Lim, S.-H., Bjorklund, T. G., Spano, F. C. & Bardeen, C. J. Exciton delocalization and superradiance in tetracene thin films and nanoaggregates. *Phys. Rev. Lett.* **92,** 107402 (2004).
30. Burdett, J. J., Gosztola, D. & Bardeen, C. J. The dependence of singlet exciton relaxation on excitation density and temperature in polycrystalline tetracene thin films: kinetic evidence for a dark intermediate state and implications for singlet fission. *J. Chem. Phys.* **135,** 214508 (2011).
31. Stern, H. L. *et al.* Identification of a triplet pair intermediate in singlet exciton fission in solution. *Proc. Natl Acad. Sci. USA* **112,** 7656–7661 (2015).
32. Mauck, C. M. *et al.* Singlet fission via an excimer-like intermediate in 3,6-bis(thiophen-2-yl)diketopyrrolopyrrole derivatives. *J. Am. Chem. Soc.* **138,** 11749–11761 (2016).

33. Korovina, N. V. *et al*. Singlet fission in a covalently linked cofacial alkynyltetracene dimer. *J. Am. Chem. Soc.* **138,** 617–627 (2016).
34. Schrauben, J. N., Ryerson, J. L., Michl, J. & Johnson, J. C. Mechanism of singlet fission in thin films of 1,3-diphenylisobenzofuran. *J. Am. Chem. Soc.* **136,** 7363–7373 (2014).
35. Ryerson, J. L. *et al*. Two thin film polymorphs of the singlet fission compound 1,3-diphenylisobenzofuran. *J. Phys. Chem. C* **118,** 12121–12132 (2014).
36. Parker, C. A. & Hatchard, C. G. Delayed fluorescence from solutions of anthracene and phenanthrene. *Proc. R. Soc. A* **269,** 574–584 (1962).
37. Odom, S. A., Parkin, S. R. & Anthony, J. E. Tetracene derivatives as potential red emitters for organic LEDs. *Org. Lett.* **5,** 4245–4248 (2003).
38. Khoury, T. & Crossley, M. J. A strategy for the stepwise ring annulation of all four pyrrolic rings of a porphyrin. *Chem. Commun.* 4851–4853 (2007).

Acknowledgements

T.W.S. acknowledges the Australian Research Council for a Future Fellowship (FT130100177). This work was supported by the Australian Research Council (Centre of Excellence in Exciton Science CE170100026, DP160103797, LE0989747).

Author contributions

C.B.D. and L.F. performed the measurements. C.B.D., J.K.G. and L.F. analysed the data. A.J.P. synthesized the TIPS-Tc material. J.E.A. designed and provided the TIPS-Tc material. M.J.C. designed and provided the $PdPQ_4$ material. T.W.S., J.K.G. and L.F. wrote the manuscript. J.K.G. and C.B.D. designed the figures with input from T.W.S. C.B.D. and P.C.T. performed the TA experiments. T.W.K. provided access to and advice on the TA experiments, and critically read the manuscript. T.W.S. conceived the experiments and performed the modelling.

Additional information

Supplementary information is available in the online version of the paper. Reprints and permissions information is available online at www.nature.com/reprints. Publisher's note: Springer Nature remains neutral with regard to jurisdictional claims in published maps and institutional affiliations. Correspondence and requests for materials should be addressed to T.W.S.

Competing financial interests

The authors declare no competing financial interests.